Dyes and Pigments 190 (2021) 109308

Contents lists available at ScienceDirect

Dyes and Pigments

journal homepage: http://www.elsevier.com/locate/dyepig

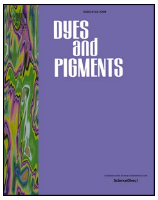

A novel porphyrin dye with phenoxazine as donor unit for efficient dye-sensitized solar cells

Shengzhong Li [a,1], Shuangyu Zhang [b,1], Shu Mei [a], Xiangfei Kong [a], Miao Yang [d], Wenjun Wu [b,*], Shuhua Zhang [c,**], Haijun Tan [a,***]

[a] *Guangxi Key Laboratory of Electrochemical and Magneto-chemical Functional Materials, College of Chemistry and Bioengineering, Guilin University of Technology, Guilin, 541004, China*
[b] *School of Chemistry and Molecular Engineering, East China University of Science & Technology, Shanghai, 200237, China*
[c] *College of Chemistry, Guangdong University of Petrochemical Technology, Maoming, Guangdong, 525000, China*
[d] *Department of Chemistry, University of Wisconsin-Madison, 1101 University Avenue, Madison, WI, 53706, United States*

ARTICLE INFO

Keywords:
Porphyrin dye
Phenoxazine
Donor unit
Dye-sensitized solar cells

ABSTRACT

A novel porphyrin dye **T-2** with phenoxazine (POZ) as donor unit has been synthesized and utilized for dye-sensitized solar cells (DSSC). Compare with porphyrin dye **T-1** (in which triphenylamine as a donor unit), the DSSC based on **T-2** exhibited a significantly higher J_{sc} (16.35 mA cm^{-2}) and V_{oc} (670 mV) than that of **T-1** (9.13 mA cm^{-2}, 610 mV), which attribute to the higher IPCE and τ of the device based on **T-2**. Correspondingly, the T-2-based device achieved a photoelectric conversion efficiency (PCE) of 7.64% (N719, 8.45%). By detailed investigation of the relationship between structure and performance, we found the butterfly-shaped structure, stronger electron-donating capability, and the extra alkyl chain of POZ are the main reasons leading to better performance of T-2 than that of T-1 in the DSSC device.

1. Introduction

Porphyrin dyes have been attracted much attention because of their excellent photovoltaic properties [1,2], and their advantages are mainly reflected in: (i) A strong light absorption capability from visible to near-infrared region, (ii) The β-position and Meso-position of the core are easy to modify, (iii) Fine-tuning of the electronic properties [3]. Since the invention of DSSC by Grätzel and co-workers in 1991, various porphyrin dyes have been synthesized and applied in DSSC [4]. Among them, **SM315** achieves a PCE of 13.0% under simulated sunlight conditions [5]. In addition, the tandem DSSC formed by the metal-free organic dye **SGT-137** (as the top battery) and porphyrin dye **SGT-021** (as the bottom battery) was proved to have an efficiency of 14.64% [6], which is extremely close to the commercialized target efficiency of 15.0%. It is well-known that rationally optimizing the molecular structure by molecular engineering can effectively improve its performance of porphyrin dyes [7]. Commonly, the design of porphyrin sensitizers often includes introducing electron-rich donors and strong electron-withdrawing acceptors to reduce the HOMO-LUMO band gap and enhance the ICT process [8]. So far, many electron-rich groups such as diphenylamine [9,10], triphenylamine [11–15], carbazole [16–18], indoline [19,20], cyanine [21,22] and phenothiazine [23–27] are widely used as electron donors in porphyrin dyes to promote the transmission and injection of electrons toward the surface of TiO$_2$. Among them, the nitrogen-anthracene electron donor has a special butterfly-shaped configuration, which is widespread adoption for DSSC [7,28,29]. Xie and co-workers synthesized a series of phenothiazine-based porphyrin sensitizers. A molecular engineering approach has also been demonstrated to improve the performance of phenothiazine-based porphyrin sensitizers. For instance, the introduction of alkyl chain into the donor (D) unit or ortho-positions of the meso-phenyl moieties is an effective way to suppress dye aggregation and charge recombination, which improves the photovoltaic behavior of DSSC [30,31]. Besides, electrochemical, photophysical, and photovoltaic investigations indicate that the introduction of additional acceptors can effectively extend the absorption spectra, resulting in better sunlight

---

* Corresponding author.
** Corresponding author.
*** Corresponding author.
E-mail addresses: wjwu@ecust.edu.cn (W. Wu), zsh720108@163.com (S. Zhang), navytan@glut.edu.cn (H. Tan).

[1] Shengzhong Li and Shuangyu Zhang contributed equally to this work.

https://doi.org/10.1016/j.dyepig.2021.109308
Received 11 February 2021; Received in revised form 10 March 2021; Accepted 10 March 2021

harvesting [32]. Recently, they reported an alternative approach for developing efficient DSSC by designing a class of “concerted companion dyes”, which achieve a remarkable efficiency of 12.4% [33]. This series of studies provide many essential strategies for the molecular engineering of porphyrin dyes. Our previous work reported that Phenoxazin, which also belongs to nitrogen anthracene, exhibits better photovoltaic performance than phenothiazine for DSSC [34].

Inspired by the discussion above, we introduced the phenoxazine as a D unit to the porphyrin dye for the first time and prepared a novel zinc porphyrin dye **T-2** (Fig. 1). In addition, we systematically analyzed the photophysical, electrochemical properties and the performance of **T-2** in DSSC. Furthermore, we simultaneously carried out a comparative analysis with **T-1** (triphenylamine (TPA) as D unit).

2. Experimental

2.1. Materials

All reagents and chemicals were purchased from Aladdin or Energy chemical reagent platform and used without further purification. All solvents were dried and freshly distilled prior to use. All column chromatographic separations were performed using Merck silica gel (60–120 mesh).

2.2. Device assembly and measurements

The procedure for preparation of TiO_2 electrodes were adapted from that reported by Grätzel and co-workers [35] and the detailed processes of device fabrication for photovoltaic measurements were very similar to the previous articles [15,36–38]. A screen-printed double layer of TiO_2 particles was used as the photoelectrode. A 12-μm thick film of 13-nm-sized TiO_2 particles was first printed on the FTO conducting glass, which was kept in a clean box for 5 min, and then dried at 125 °C over 6 min, and further coated by a 5-μm thick second layer of 400-nm light-scattering anatase particles. Finally, the electrodes coated with the TiO_2 pastes were gradually sintered in a muffle furnace at 275 °C for 5 min, at 325 °C for 5 min, at 375 °C for 5 min, at 450 °C for 15 min and at 500 °C for 15 min, respectively. The size of the TiO_2 film was 0.25 cm^2. These films were immersed into a 40 mM aqueous $TiCl_4$ solution at 70 °C for 30 min, washed with water and ethanol, and then heated again at 450 °C for 30 min. The films were then immersed into a 300 μM solution of **T-1** or **T-2** in a mixture of chloroform and ethanol (volume ratio of 3 : 7) for 10 h at room temperature. The seal uses a 45 mm thick Bynel (DuPont) hot melt gasket to fill the electrolyte into the interior space through a vacuum backfill system. The osmotic electrolyte consisted: 0.6 M dimethylpropylimidazolium iodide, 0.05 M I2, 0.1 M LiI, and 0.5 M tert-butylpyridine in acetonitrile. 4 parallel cells for each dye molecule will be prepared to obtain more reasonable and credible data. Under standard AM 1.5 simulated solar irradiation (WXS155S-10), photocurrent density-voltage (J−V) curves of solar cell devices were measured by Keithley 2400 Source Meter Instruments. Monochromatic incident photon-to-current conversion efficiency (IPCE) spectra measurement was performed by a Newport-74125 system (Newport Instruments). Electrochemical impedance spectroscopy (EIS) was measured with a two-electrode system in the dark by Electrochemical Workstation (Zahner IM6e) [39].

3. Results and discussion

3.1. Dye structures and syntheses

The synthesis of dyes **T-1** and **T-2** are summarized in Scheme 1. The POZ was synthesized following our published procedure [34], porphyrin core, and the A-π-A unit was synthesized via procedures from the literature [30,40]. The synthetic details are shown in Scheme S1, and the results of intermediates are provided in the Supporting.

Compound 11. Compound **5** (0.75 g, 0.53 mmol), compound **10** (0.12 g, 0.42 mmol), $Pd_2(dba)_3$ (0.19 g, 0.21 mmol) and $AsPh_3$ (0.28 g, 0.90 mmol) were dissolved in THF (60 mL) and Et_3N (20 mL). After the solution was stirred at 55 °C under argon for 6 h. The solvent was removed under reduced pressure and the residue was purified by column chromatography on silica gel using petroleum ether/CH_2Cl_2 (1:1, v:v) to give compound **11** as green powders (0.22 g, yield: 25.5%). ^1H NMR ($CDCl_3$, 500 MHz, ppm) δ 10.03–10.01 (d, 2H), 9.63–9.60 (d, 2H), 9.00–8.98 (d, 2H), 8.88–8.87 (d, 2H), 8.18–8.16 (d, 1H), 8.09–8.06 (d, 2H), 7.99–7.95 (d, 2H), 7.76–7.73 (s, 3H), 7.08–7.04 (d, 4H), 4.01–3.98 (s, 3H), 3.92–3.89 (m, 8H), 1.35–1.02 (m, 28H), 1.01–0.88 (m, 18H), 0.86–0.74 (m, 20H), 0.65–0.35 (m, 26H). MS: $m/z = 1633.77$.

Compound 13a. Compound **11** (83.00 mg, 0.05 mmol), compound **12a** (0.25 g, 0.10 mmol) and CH_3COOK (14.70 mg, 0.15 mmol) were dissolved in THF/H_2O (33 mL, 10/1, v/v) and $Pd(pph_3)_4$ (115.56 mg, 0.10 mmol) were added at 70 °C under argon for 12 h. Then the solvent was removed under reduced pressure, and the residue was dissolved in CH_2Cl_2 and washed with water, dried over anhydrous Na_2SO_4 and evaporated. The residue was purified by column chromatography on silica gel using petroleum ether/CH_2Cl_2 (1:1, v:v) to give compound **13a** as green powders (74.30 mg, yield: 82.7%). ^1H NMR ($CDCl_3$, 500 MHz, ppm) δ 10.16–10.13 (d, 1H), 10.11–10.09 (d, 1H), 9.28–9.24 (d, 1H), 9.12–9.07 (d, 1H), 9.06–9.03 (d, 1H), 9.00–8.97 (d, 1H), 8.96–8.92 (d, 1H), 8.88–8.85 (d, 1H), 8.33–8.28 (t, 1H), 8.07–8.21 (t, 2H), 8.18–8.15 (d, 1H), 8.09–8.04 (d, 1H), 7.96–7.90 (t, 1H), 7.76–7.70 (t, 2H), 7.43–7.41 (d, 4H), 7.34–7.31 (d, 1H), 7.24–7.20 (t, 2H), 7.17–7.12 (t, 2H), 7.08–7.06 (d, 2H), 7.05–7.04 (d, 2H), 4.03–4.00 (s, 3H), 3.93–3.84 (m, 8H), 1.25–1.12 (m, 10H), 1.08–0.97 (m, 20H), 0.93–0.86 (m, 10H), 0.84–0.77 (m, 24H), 0.70–0.62 (m, 8H), 0.61–0.47 (m, 16H), 0.46–0.38 (m, 8H).MS: $m/z = 1796.97$.

Dye T-1. Compound **13a** (74.30 mg, 41.35 μmol) and $LiOH{\cdot}H_2O$ (69.40 mg, 1.65 mmol) were dissolved in THF (30 mL) and H_2O (2 mL), respectively. Then the mixed solution was stirred at 55 °C under argon for 6 h. Then the solvent was removed under reduced pressure, and the residue was dissolved in CH_2Cl_2 and washed with water, dried over anhydrous Na_2SO_4 and evaporated. The residue was purified by column chromatography on silica gel using CH_2Cl_2/MeOH (20:1, v:v) to give **T-1** as green powders (64.95 mg, yield: 88.1%). ^1H NMR ($CDCl_3$, 500 MHz,

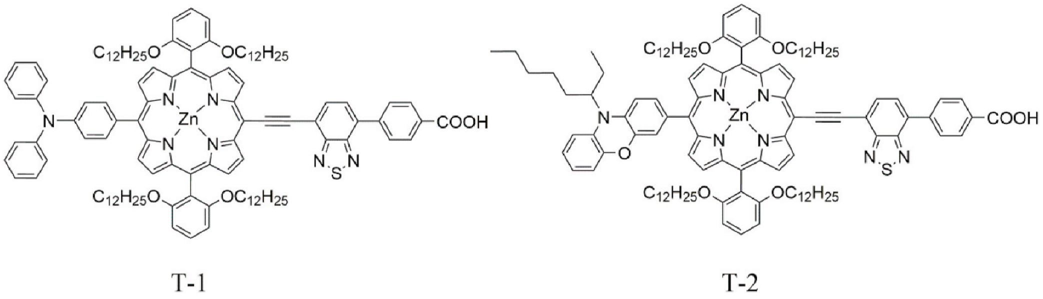

Fig. 1. Molecular structures of the **T-1** and **T-2**.

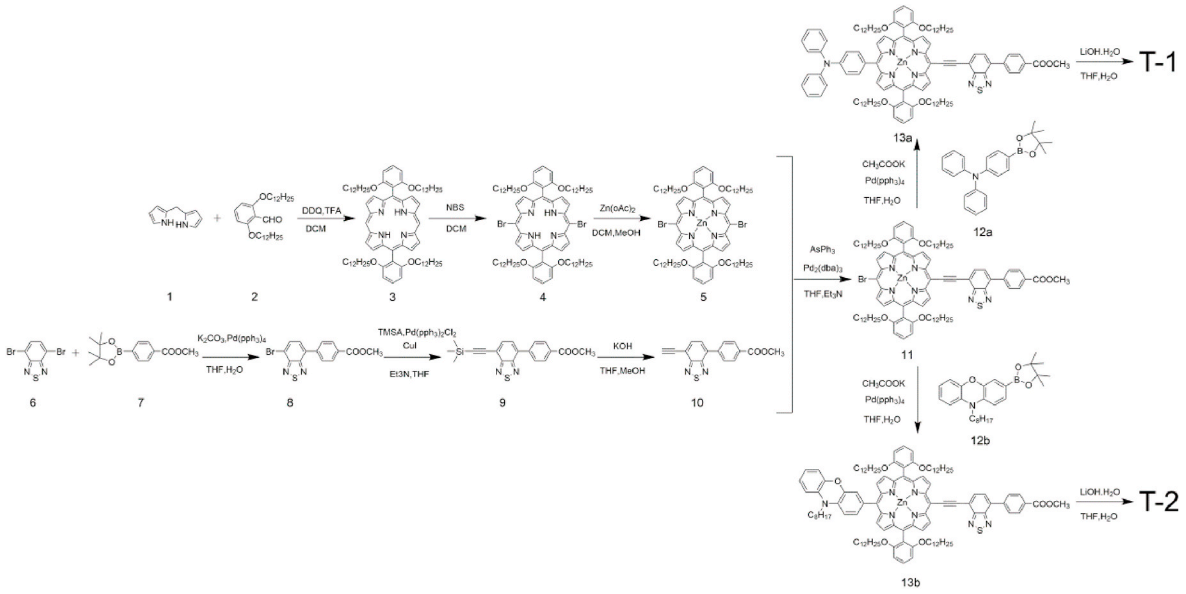

Scheme 1. Synthetic routes of **T-1** and **T-2**.

ppm) δ 10.12–10.09 (d, 1H), 10.07–10.03 (d, 1H), 9.05–9.03 (d, 1H), 9.02–9.00 (d, 1H), 8.99–8.96 (d, 1H), 8.95–8.93 (d, 1H), 8.90–8.85 (m, 2H), 8.30–8.26 (d, 1H), 8.25–8.20 (d, 2H), 8.16–8.10 (d, 3H), 8.09–8.03 (d, 2H), 7.93–7.86 (t, 2H), 7.79–7.70 (m, 4H), 7.42–7.38 (m, 6H), 7.08–7.02 (m, 6H), 3.91–3.87 (t, 8H), 1.25–1.12 (m, 10H), 1.08–0.97 (m, 20H), 0.93–0.86 (m, 10H), 0.84–0.77 (m, 20H), 0.70–0.62 (m, 8H), 0.61–0.47 (m, 16H), 0.46–0.38 (m, 8H). MS: $m/z = 1782.95$.

Compound 13b. Compound **13b** was synthesized following the same procedure as that for compound **13a**, except that compound **12b** (0.25 g, 0.60 mmol) was used instead of compound **12a**. Green powders, yield: 48.76 mg, 87.9%. ^{1}H NMR ($CDCl_3$, 500 MHz, ppm) δ 10.18–10.13 (d, 2H), 9.20–9.14 (d, 1H), 9.07–9.03 (m, 3H), 8.99–8.94 (d, 1H), 8.86–8.84 (d, 1H), 8.35–8.32 (d, 1H), 8.30–8.27 (d, 2H), 8.22–8.19 (d, 2H), 8.01–7.95 (t, 3H), 7.78–7.73 (d, 1H), 7.40–7.35 (d, 1H), 7.08–7.04 (d, 2H), 6.92–6.88 (d, 2H), 6.75–6.71 (d, 3H), 6.66–6.63 (d, 1H), 6.56–6.53 (d, 1H), 4.03–4.02 (s, 3H), 3.97–3.76 (m, 8H), 2.07–2.02 (m, 1H), 1.35–1.25 (m, 46H), 0.93–0.88 (m, 15H), 0.82–0.77 (m, 15H), 0.70–0.61 (m, 8H), 0.55–0.43 (m, 16H). MS: $m/z = 1847.04$.

Dye T-2. T-2 was synthesized following the same procedure as that for **T-1**, except that compound **13b** (48.76 mg, 26.37 μmol) was used instead of compound **13a**. Green powders, yield: 41.47 mg, 85.7%. ^{1}H NMR ($CDCl_3$, 500 MHz, ppm) δ 10.17–10.13 (d, 1H), 10.11–10.07 (d, 1H), 9.07–9.02 (d, 2H), 9.02–8.99 (t, 1H), 8.98–8.94 (d, 1H), 8.89–8.80 (m, 2H), 8.35–8.27 (m, 3H), 8.22–8.20 (d, 1H), 8.02–7.94 (m, 2H), 7.77–7.70 (m, 2H), 7.60–7.54 (t, 1H), 7.53–7.47 (t, 1H), 7.22–7.18 (d, 1H), 7.06–7.01 (d, 2H), 6.91–6.88 (d, 1H), 6.75–6.69 (d, 3H), 6.67–6.64 (d, 1H), 6.58–6.53 (d, 1H), 3.99–3.78 (t, 8H), 1.97–1.91 (m, 1H), 1.35–1.25 (m, 46H), 0.93–0.88 (m, 15H), 0.82–0.77 (m, 15H), 0.70–0.61 (m, 8H), 0.55–0.43 (m, 16H). MS: $m/z = 1833.03$.

3.2. Optical properties

Fig. 2 shows the UV–vis absorption spectra of **T-1** and **T-2** in the tetrahydrofuran (THF) solution. Table 1 summarize their corresponding absorption maxima (λ_{max}^{abs}) and molar absorptivity (ε) of Soret and Q bands. These porphyrin dyes exhibit an intensive Soret band at 400–550 nm (**T-1**, $\lambda_{max}^{abs} = 433$ nm, $\varepsilon = 105869.25$ M^{-1} cm^{-1}; **T-2**, $\lambda_{max}^{abs} = 431$ nm; $\varepsilon = 115{,}595$ M^{-1} cm^{-1}), due to the characteristic π–π* transition localized mainly at the porphyrin core. A moderate Q-band at 600–750 nm (**T-1** $\lambda_{max}^{abs} = 648$ nm, $\varepsilon = 36702.25$ M^{-1} cm^{-1}; **T-2**$\lambda_{max}^{abs} = 645$ nm, $\varepsilon = 37861.5$ M^{-1} cm^{-1}), which is attributed to π–π* charge-transfer transitions of the conjugated molecule and intramolecular charge transfer from the donor unit to the acceptor unit of dyes. Our spectral test results show that the two dyes have almost the same spectral

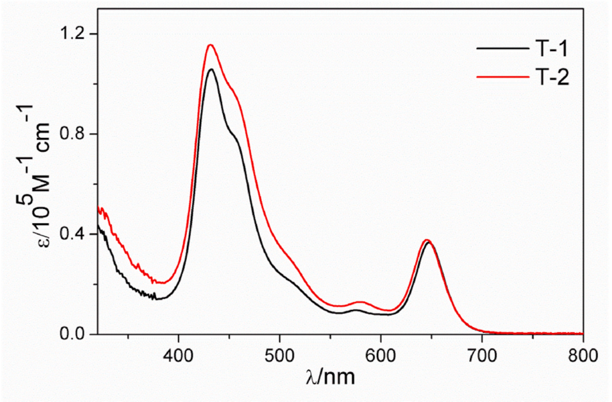

Fig. 2. UV–vis absorption spectra of **PTZ-3** and **PTZ-5** in THF.

Table 1
Photophysical and electrochemical date of **T-1** and **T-2**.

dye	λ_{max}^{abs} [a] /nm	ε_{max}^{abs} [a] /$M^{-1}cm^{-1}$	λ_{max}^{pl} [a] /nm	E_{0-0} [b] /eV	E_{OX} [c] /V	E_{OX}^{*} [d] /V
T-1	433 648	1.05969.25 36702.25	711	1.84	0.61	−1.23
T-2	431 645	115,595 37861.5	708	1.85	0.63	−1.22

[a] The maximum absorption wavelength (λ_{max}^{abs}), the maximum molar absorption coefficient (ε_{max}^{abs}) and the maximum emission wavelength (λ_{max}^{pl}) were derived from the steady-state absorption-emission spectra of the dye in THF. The molar absorption coefficient(ε) were calculated by the equation $\varepsilon = A/(cl)$, where A is absorbance, c is concentration in moles per liter and l is path length in centimeters.

[b] The 0-0 transition energy ($E_{0\text{-}0}$) was estimated from the intersection of the normalized absorption and emission spectra.

[c] The ground state redox electricity (E_{OX}) was referenced to Fc^+/Fc.

[d] The excited redox potential (E_{OX}^{*}) was derived from the formula $E_{OX}^{*} = E_{OX} - E_{0-0}/e$ without considering the entropy change in the light excitation process.

response range, and the ε of **T-2** is slightly higher than that of **T-1**, especially in the range of 400–600 nm. Moreover, the steady-state emission spectra of **T-1** and **T-2** dyes were measured in THF and are shown in Fig. S12 and Table 1. The optical band gap width (E_{0-0}) can be estimated from the intersections of the normalized UV–visible absorption spectrum and emission spectrum, as shown in Fig. 3. According to the transition bandgap formula: $E_{0-0} = 1240/\lambda$, the calculated E_{0-0} of **T-1** and **T-2** are 1.84 and 1.85 eV, respectively.

3.3. Electrochemical properties

To obtain the electrochemical properties of **T-1** and **T-2,** we conducted measurements using cyclic voltammetry (CV). Table 1 and Fig. 4 summarize the CV results of **T-1** and **T-2**. Both **T-1** and **T-2** exhibit reversible waves for the first oxidation peaks (E_{OX}), corresponding to the HOMO of the dye and indicating that oxidation happens at the donor. The estimated ground state oxidation potentials E_{OX} of **T-1** and **T-2** are 0.61 and 0.63 V, respectively, versus the normal hydrogen electrode (NHE). Hence, both T-1 and T-2 show sufficiently higher potentials than the I^-/I_3^- redox electrolyte (0.4 V) redox couple, indicating enough driving force for regenerating the oxidized dyes by I^-/I_3^- redox electrolytes. The expression $E^*_{OX} = E_{OX} - E_{0-0}/e$ was used to calculate the excited state oxidation potential (E^*_{OX}) of **T-1** and **T-2**, and the corresponding values are -1.71 and -1.70 V, respectively. Thus, there are enough driving forces for injecting electrons from **T-1** and **T-2** into the conduction band edge (E_{CB}) of TiO_2 (-0.5 V) (Fig. 5).

3.4. Theoretical calculations

To gain insight into the molecular structures as well as the influence of different substituents on the electron distribution of dyes **T-1** and **T-2**, we performed DFT and TD-DFT calculations using the functional basis set B3LYP/6-31G(d, p). Figs. 6 and 7 show the optimized molecular structure and frontier molecular orbitals (FMOs) of **T-1** and **T-2** dyes. As shown in Fig. 7, the HOMO orbitals are mainly distributed in the donor unit and the porphyrin macrocycle. In contrast, the LUMO orbitals are predominantly delocalized over the acceptor unit and the porphyrin macrocycle. This distribution means that the electrons can be effectively transported from the HOMO orbital to the LUMO orbital. In other words, the electronic transfer process from the donor to the benzoic acid acceptor can be easily transported, followed by facilitating the electron injection from the dyes to the TiO_2 surface. The simulated UV–vis absorption spectra of the dyes in THF solvent are presented in Fig. S13 and the corresponding data are collected in Table S1. The intense Soret band around 450 nm and moderate Q-band around 600 nm corresponds to the local excitation of the zinc-porphyrin and intramolecular charge transfer, respectively, which are very consistent with our spectral test results.

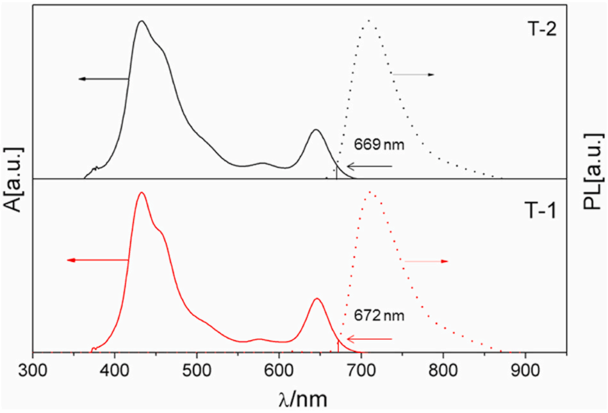

Fig. 3. Normalized electronic absorption and emission spectra of the **T-1** and **T-2** in THF.

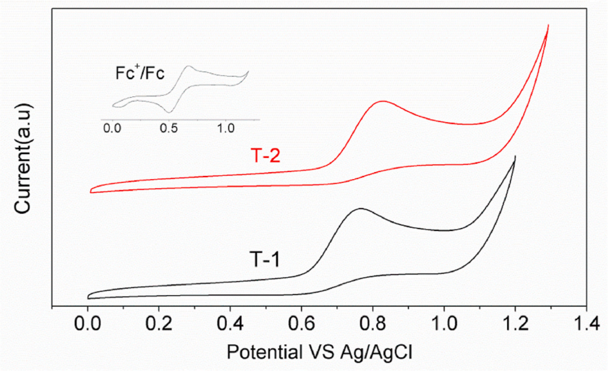

Fig. 4. Cyclic voltammetry of **T-1** and **T-2** in THF.

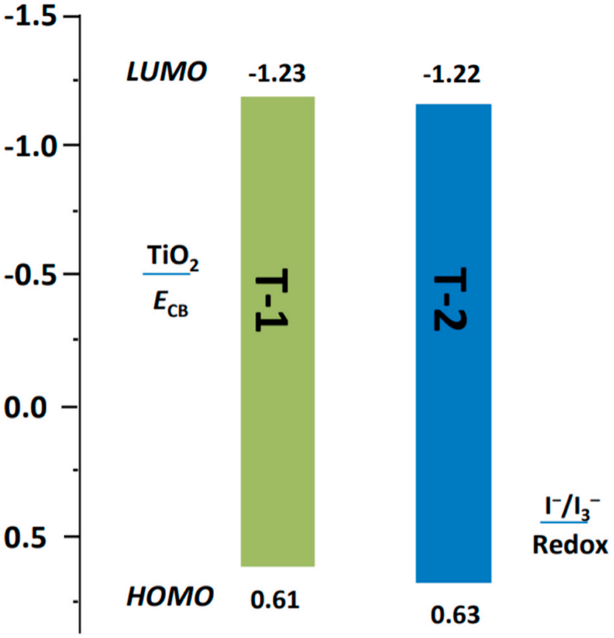

Fig. 5. Energy diagrams of **T-1** and **T-2**.

3.5. Photovoltaic performance of DSSC

The dyes were used to fabricate DSSC, and the corresponding photovoltaic parameters are summarized in Table 2. Figs. 8 and 9 show the photocurrent−voltage curves (*J-V*) and the incident photon-to-current conversion efficiency (IPCE) action spectra. Both T1 and T2 show a broad IPCE action spectrum from 300 nm to 800 nm, suggesting that they can effectively convert visible light into photocurrent. The IPCE values of **T-2** are significantly higher than those of **T-1**, which is mainly attributed to the higher ε of **T-2** and the extra alkyl chain on POZ, which can suppress the recombination of interfacial electrical to reduce the dark current. Therefore, **T-2** exhibited higher IPCE and short-circuit current density (J_{sc}) values of 16.35 mA cm^{-2}. Open-circuit voltage (V_{oc}) is also an essential parameter for DSSC. Compared with **T-1** ($V_{oc} = 610$ mV; PCE $= 4.12\%$), **T-2** exhibited higher V_{oc} of 670 mV and PCE of 7.64%.

3.6. Electrochemical impedance spectroscopy

To further understand the photovoltaic behavior of DSSC based on these two dyes, we performed electrochemical impedance spectroscopy (EIS) in the dark. As we all know, the V_{oc} of DSSC represents the potential difference between the quasi-Fermi level (E_f) of TiO_2 and the

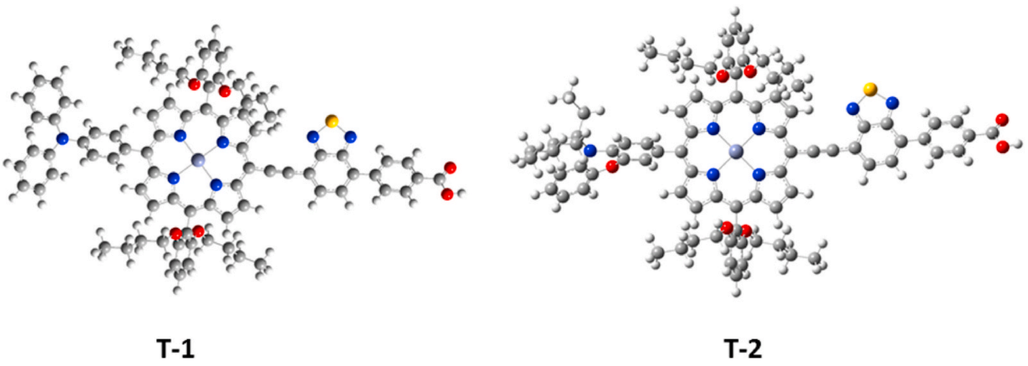

Fig. 6. Simulated optimized structure structure of dyes.

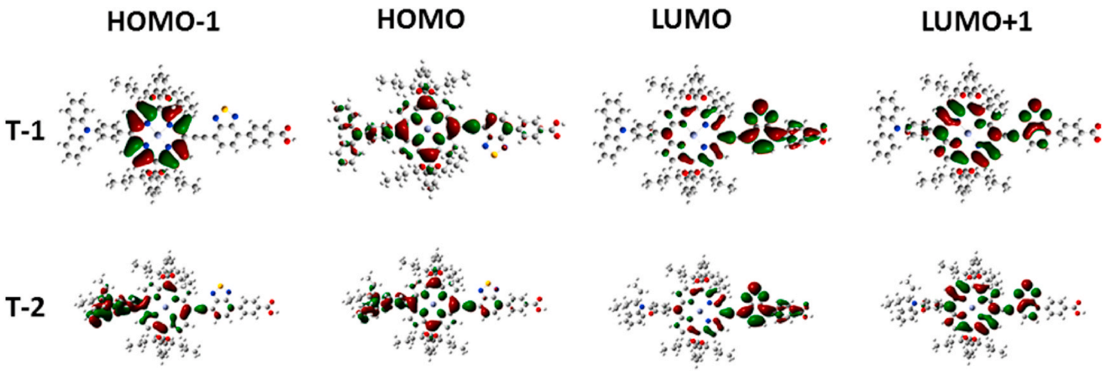

Fig. 7. Electron cloud distribution of dyes at the B3LYP/6-31G(d,p) level with Gaussian09.

Table 2
Photovoltaic parameters of cells measured at an irradiation of 100 mW cm^{-2}, simulated AM 1.5 sunlight.

dyes	V_{oc}/V	J_{sc}/mA·cm^{-2}	FF%	PCE%
T-1	0.61 ± 0.03	9.13 ± 0.66	73.45 ± 4.62	4.12 ± 0.28
T-2	0.67 ± 0.01	16.35 ± 1.90	70.13 ± 0.7	7.64 ± 0.69
N719	0.71	16.92	70.45	8.45

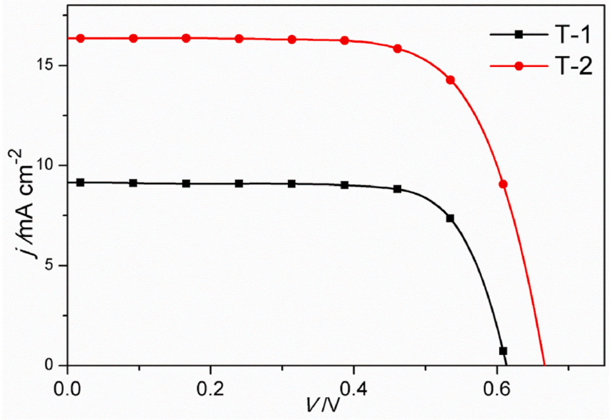

Fig. 8. *J–V* characteristics measured under irradiation of 100 mW cm^{-2} simulated AM 1.5 sunlight.

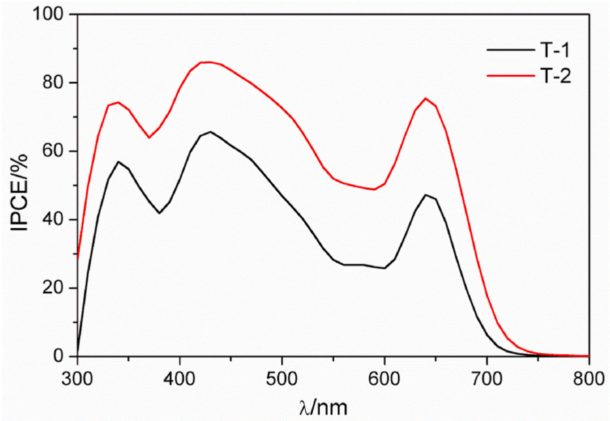

Fig. 9. Incident photon-to-electron conversion efficiency (IPCE) spectra of the dyes **T-1** and **T-2**.

redox electrolyte. Since the redox electrolyte is fixed in the experiment, the change of V_{oc} is related to the value of E_f, which can be inferred from the chemical capacitance (C_μ). Besides, V_{oc} is in connection with electron lifetime (τ), which can reflect the injected electron density. As shown in Fig. 10a, the C_μ of the **T-1** and **T-2** DSSCs are almost identical, which indicates a negligible impact of the conduction band position of TiO_2 on V_{oc} variation. In addition, the dependence of electron lifetimes (τ) on bias voltage is plotted in Fig. 10b. In general, a longer electron lifetime implies a slower charge recombination rate at the dye-sensitized TiO_2—electrolyte interface. The longer τ of **T-2** causing higher injected electron density (Fig. 10b), which is consistent with that of V_{oc}, ranking as **T-1** < **T-2**. These results indicate that the charge recombination process determined the V_{oc} values of DSSC.

4. Conclusions

In summary, a novel porphyrin sensitizer (**T-2**) containing a

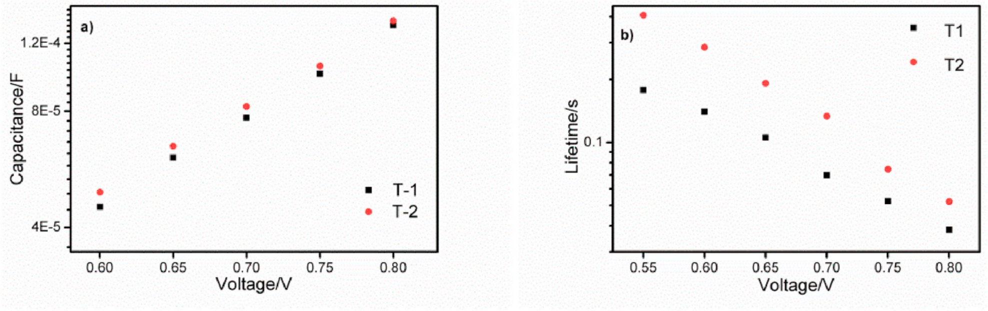

Fig. 10. TiO_2 capacitance (a) and electron lifetime (b) as a function of potential based on dyes **T-1** and **T-2**.

phenoxazine (POZ) as an electron donor has been designed and synthesized for DSSC. Compared to T-1 with triphenylamine donor unit, T-2 exhibits higher efficiency of 7.64% due to the distinctive structure and strong electron-donating capability of POZ. Our results indicate that POZ is a very promising donor unit for developing high-efficiency porphyrin dyes for DSSC.

Author contribution statement

Shengzhong Li: Synthesized and characterized the dyes, Writing-original draft. **Shuangyu Zhang:** Device fabrication and performance measurement. **Shu Mei:** Data curation. **Xiangfei Kong:** Investigation. **Miao Yang:** Formal analysis, Writing-review. **Wenjun Wu:** Device studies, Formal analysis, Data curation. **Shuhua Zhang:** DFT Calculation, Formal analysis. **Haijun Tan:** Conceptualization, Supervision, Funding acquisition, Writing-review & editing.

Declaration of competing interest

The authors declare that they have no known competing financial interests or personal relationships that could have appeared to influence the work reported in this paper.

Acknowledgements

This work was supported by grants from the National Natural Science Foundation of China (NSFC 21663010), Natural Science Foundation of Guangxi, China (2015GXNSFBA139029), the special funding for distinguished experts from Guangxi Zhuang Autonomous Region.

Appendix A. Supplementary data

Supplementary data to this article can be found online at https://doi.org/10.1016/j.dyepig.2021.109308.

References

[1] Urbani M, Grätzel M, Nazeeruddin MK, Torres T. Meso-substituted porphyrins for dye-sensitized solar cells. Chem Rev 2014;114:12330–96.
[2] Li LL, Diau WG. Porphyrin-sensitized solar cells. Chem Soc Rev 2013;42:279–317.
[3] Ji JM, Kim SH, Zhou H, Kim CH, Kim HK. D-π-A-structured porphyrins with extended auxiliary π-spacers for highly efficient dye-sensitized solar cells. ACS Appl Mater Interfaces 2019;11:24067–77.
[4] O'Regan B, Grätzel M. A Low-cost, high-efficiency solar cell based on dye-sensitized colloidal TiO_2 films. Nature 1991;353:737–40.
[5] Mathew S, Yella A, Gao P, Humphry-Baker R, Curchod BFE, Ashari-Astani N, et al. Dye-sensitized solar cells with 13% efficiency achieved through the molecular engineering of porphyrin sensitizers. Nat Chem 2014;6:242–7.
[6] Eom YK, Kang SH, Choi IT, Yoo Y, Kim J, Kim HK. Significant light absorption enhancement by a single heterocyclic unit change in the π-bridge moiety from thieno[3, 2-b]benzothiophene to thieno[3, 2-b]indole for high performance dye-sensitized and tandem solar cells. J Mater Chem 2017;5:2297–308.
[7] Zeng K, Tong Z, Ma L, Zhu WH, Wu W, Xie Y. Molecular engineering strategies for fabricating efficient porphyrin-based dye-sensitized solar cells. Energy Environ Sci 2020;13:1617–57.
[8] Song H, Liu Q, Xie Y. Porphyrin-sensitized solar cells: systematic molecular optimization, coadsorption and cosensitization. Chem Commun 2018;54:1811–24.
[9] Hsueh-Pei Lu, Chi-Lun Mai, Chen-Yuan Tsia, et al. Design and characterization of highly efficient porphyrin sensitizers for green see-through dye-sensitized solar cells. Phys Chem Chem Phys 2009;11:10270–4.
[10] Wang C-L, Zhang M, Hsiao Yu-Hsin, Tseng Chuan-Kai, Chia-Lin Liu, Xu M, et al. Porphyrins bearing a consolidated anthryl donor with dual functions for efficient dye-sensitized solar cells. Energy Environ Sci 2016;9:200–6.
[11] Yum JH, Hagberg DP, Moon SJ, Karlsson KM, Marinado T, Sun L, et al. Light-resistant organic sensitizer for solar-cell applications. Angew Chem Int Ed Engl 2009;48:1576–80.
[12] He J, Wu W, Hua J, Jiang Y, Qu S, Li J, et al. Bithiazole-bridged dyes for dye-sensitized solar cells with high open circuit voltage performance. J Mater Chem 2011;21:6054–62.
[13] Wu W, Zhang J, Yang H, Jin B, Hu Y, Hua J, et al. Narrowing band gap of platinum acetylide dye-sensitized solar cell sensitizers with thiophene π-bridges. J Mater Chem 2012;22:5382–9.
[14] Mizuno Y, Yisilamu Y, Yamaguchi T, Tomura M, Funaki T, Sugihara H, et al. (Dibenzoylmethanato)boron difluoride derivatives containing triphenylamine moieties: a new type of electron-donor/π-acceptor system for dye-sensitized solar cells. Chem Eur J 2014;20:13286–95.
[15] Tang Y, Wang Y, Li X, Agren H, Zhu WH, Xie Y. Porphyrins containing a triphenylamine donor and up to eight alkoxy chains for dye-sensitized solar cells: a high efficiency of 10.9%. ACS Appl Mater Interfaces 2015;7:27976–85.
[16] Koumura N, Wang Z-S, Miyashita M, Uemura Y, Sekiguchi H, Cui Y, et al. Substituted carbazole dyes for efficient molecular photovoltaics: long electron lifetime and high open circuit voltage performance. J Mater Chem 2009;19:4829–36.
[17] Luo C, Bi W, Deng S, Zhang J, Chen S, Li B, et al. Indolo[3, 2, 1-jk]carbazole derivatives-sensitized solar cells: effect of π-bridges on the performance of cells. J Phys Chem C 2014;118:14211–7.
[18] Su JY, Lo CY, Tsai CH, Chen CH, Chou SH, Liu SH, et al. Indolo[2,3-b]carbazole synthesized from a double-intramolecular buchwald-hartwig reaction: its application for a dianchor dssc organic dye. Org Lett 2014;16:3176–9.
[19] Horiuchi T, Miura H, Sumioka K, Uchida S. High efficiency of dye-sensitized solar cells based on metal-free indoline dyes. J Am Chem Soc 2004;126:12218–9.
[20] Cabau L, Pelleją L, Clifford JN, Kumar CV, Palomares E. Light soaking effects on charge recombination and device performance in dye sensitized solar cells based on indoline-cyclopentadithiophene chromophores. J Mater Chem 2013;1:8994–9000.
[21] Funabiki K, Mase H, Hibino A, Tanaka N, Mizuhata Sakuragi. Synthesis of a novel heptamethine-cyanine dye for use in near-infrared active dye-sensitized solar cells with porous zinc oxide prepared at low temperature. Energy Environ 2011;4:2186–92.
[22] Tang J, Wu W, Hua J, Li J, Li X, Tian H. Starburst triphenylamine-based cyanine dye for efficient quasi-solid-state dye-sensitized solar cells. Energy Environ Sci 2009;2:982–90.
[23] Venkatraman V, Alsberg BRKR. A quantitative structure-property relationship study of the photovoltaic performance of phenothiazine dyes. Dyes Pigments 2015;114:69–77.
[24] Wu W, Yang J, Hua J, Jin T, He T. Efficient and stable dye-sensitized solar cells based on phenothiazine sensitizers with thiophene units. J Mater Chem 2010;20:1772–9.
[25] Hua Y, Chang S, He J, Zhang C, Zhao J, Chen T, et al. Molecular engineering of simple phenothiazine-based dyes to modulate dye aggregation, charge recombination, and dye regeneration in highly efficient dye-sensitized solar cells. Chem Eur J 2014;20:6300–8.
[26] Sun X, Wang Y, Li X, Agren H, Zhu W, Tian H, et al. Cosensitizers for simultaneous filling up of both absorption valleys of porphyrins: a novel approach for developing efficient panchromatic dye-sensitized solar cells. Chem Commun 2014;50:15609–12.
[27] Hua Y, Chang S, Huang D, Zhou X, Zhu X, Zhao J, et al. Significant improvement of dye-sensitized solar cell performance using simple phenothiazine-based dyes. Chem Mater 2013;25:2146–53.
[28] Zeng K, Tang W, Li C, Chen Y, Zhao S, Liu Q, et al. Systematic optimization of the substituents on the phenothiazine donor of doubly strapped porphyrin sensitizers:

an efficiency over 11% unassisted by any cosensitizer or coadsorbent. J Mater Chem 2019;7:20854–60.

[29] Kumar R, Sudhakar V, Prakash K, Krishnamoorthy K, Sankar M. Tuning the photovoltaic performance of dsscs by appending various donor groups on trans-dimesityl porphyrin backbone. ACS Appl Energy Mater 2018;1:2793–801.

[30] Song H, Li X, Ågren H, Xie Y. Branched and linear alkoxy chains-wrapped push-pull porphyrins for developing efficient dye-sensitized solar cells. Dyes Pigments 2017; 137:421–9.

[31] Lu Y, Song H, Li X, Agren H, Liu Q, Zhang J, et al. Multiply wrapped porphyrin dyes with a phenothiazine donor: a high efficiency of 11.7% achieved through a synergetic coadsorption and cosensitization approach. ACS Appl Mater Interfaces 2019;11:5046–54.

[32] Pan J, Song H, Lian C, Liu H, Xie Y. Cocktail co-sensitization of porphyrin dyes with additional donors and acceptors for developing efficient dye-sensitized solar cells. Dyes Pigments 2017;140:36–46.

[33] Zeng K, Chen Y, Zhu WH, Tian H, Xie Y. Efficient solar cells based on concerted companion dyes containing two complementary components: an alternative approach for cosensitization. J Am Chem Soc 2020;142:5154–61.

[34] He J, Pei H, Li H, Zhang S, Zhang S, Tan H, et al. Comparative analysis of phenothiazine and phenoxazine sensitizers for dye-sensitized solar cells. Syn. Met 2019;247:228–32.

[35] Ito S, Murakami TN, Comte P, Liska P, Grätzel C, Nazeeruddin MK, et al. Fabrication of thin film dye sensitized solar cells with solar to electric power conversion efficiency over 10%. Thin Solid Films 2008;516:4613–9.

[36] Liu J, Liu B, Tang Y, Zhang W, Wu W, Xie Y, et al. Highly efficient cosensitization of D-A-π-A benzotriazole organic dyes with porphyrin for panchromatic dye-sensitized solar cells. J Mater Chem C 2015;3:11144–50.

[37] Wang Y, Zheng Z, Li T, Robertson N, Xiang H, Wu W, et al. D-A-π-A motif quinoxaline-based sensitizers with high molar extinction coefficient for quasi-solid-state dye-sensitized solar cells. ACS Appl Mater Interfaces 2016;8:31016–24.

[38] Wang Y, Chen B, Wu W, Li X, Zhu W, Tian H, et al. Efficient solar cells sensitized by porphyrins with an extended conjugation framework and a carbazole donor: from molecular design to cosensitization. Angew Chem Int Ed Engl 2014;53:10779–83.

[39] Jiang H, Wu Y, Islam A, Wu M, Zhang W, Shen C, et al. Molecular engineering of quinoxaline-based D-A-π-A organic sensitizers: taking the merits of a large and rigid auxiliary acceptor. ACS Appl Mater Interfaces 2018;10:13635–44.

[40] Song H, Tang W, Zhao S, Liu Q, Xie Y. Porphyrin sensitizers containing an auxiliary benzotriazole acceptor for dye-sensitized solar cells: effects of steric hindrance and cosensitization. Dyes Pigments 2018;155:323–31.